Diffusion processes relevant to homoepitaxial growth on Ag(100)

Ulrike Kürpick and Talat. S. Rahman
Department of Physics, Cardwell Hall 116, Kansas State University, Manhattan, Kansas 66506
(Received 10 June 1997)

We present results of theoretical calculations of activation barriers and preexponential factors for several diffusion processes that are involved in interlayer and intralayer transport on Ag(100). The thermodynamic functions necessary for the evaluation of the diffusion coefficients for adatom diffusion via hopping and exchange on a flat Ag(100) surface, and on that with a ⟨110⟩, and a ⟨100⟩ step edge, exhibit their explicit dependence on the local vibrational density of states. On the flat surface, hopping is found to be favored at low temperatures, while inclusion of bulk thermal expansion makes exchange processes competitive at higher temperatures. We show for the first time that the dominant path for interlayer transport on Ag(100) is via exchange over the ⟨100⟩-step edge with a negative Ehrlich-Schwoebel barrier and discuss the consequences of the relatively high barrier for adatom mobility along the ⟨100⟩-step edge, as compared to that along the ⟨110⟩. [S0163-1829(98)05003-6]

I. INTRODUCTION

There continues to be considerable interest in the phenomenon of epitaxial growth since it offers unique opportunities for a fundamental understanding of the nature of bonding at surfaces while at the same time exploring ways to control and improve the production of materials with desirable properties. One of the factors controlling epitaxial growth is the mobility of adatoms on flat terraces, and on or near steps that are inevitably present on surfaces. The character of the growth process, i.e., whether it is two dimensional and progressing layer by layer, or three dimensional and proceeding in the form of separated clusters, depends strongly on the intralayer and interlayer mobility of the adatoms. If the adatoms can descend easily from an island to a lower surface plane the growth is likely to be layer by layer. If, on the other hand, there is a barrier to such a descent, the Ehrlich-Schwoebel barrier[1] as illustrated in Fig. 1, the growth is likely to proceed with formations of three-dimensional clusters. From observations on a few (100) and (111) surfaces of transition metals, it may appear that the growth is layer by layer on (100) and via 3D clusters on (111), but the picture is far from being universal. While homoepitaxy experiments on Ag(100) (Refs. 2, 3) and Ag(111) (Refs. 2–6) do conform to this particular view, and the observed multilayer growth on Ag(111) can be explained by the existence of an Ehrlich-Schwoebel barrier of 150 meV,[5,7] similar experiments on Pt(111), and on Cu(100) and Cu(111), reveal a more complex growth pattern.[8]

In the case of two-dimensional growth, the shape of the islands, in turn, depends on the mobility of the adatom along the step edges. High mobility leads to smooth step edges, and low mobility results in rough or fractal-like edges. While it is easy to understand the direct dependence of mobility on surface temperature, and hence the presence of fractal-like step edges at low temperatures and smoother ones at higher temperatures, the temperature dependence of the shapes of the smooth edged, two-dimensional islands is not so obvious. At these higher temperatures the relative mobility of the adatom along different types of step edges may be expected to control the shapes of the islands and growth processes.[8] In order to understand the microscopic factors responsible for the temperature-dependent relative mobility along steps of different orientations, we need reliable information about the diffusion coefficients for relevant paths and processes. We have recently developed a theoretical framework for calculating such diffusion coefficients, using transition-state theory[9] and exploiting the differences in the vibrational free energy content of the system when the adatom is at the saddle point and when it is at the minimum-energy configurations.[10,11] As special applications to the case of self diffusion via hopping on Ag(100), Cu(100), and Ni(100), we have shown that through inclusion of vibrational free-energy contributions the temperature-dependent diffusion coefficient can be extracted quite reliably, and that the calculated preexponential factors are in quite good agreement with those that have been either assumed or extracted from the analyses of experimental data. For these cases, we have also found the activation barriers for hopping to be affected by the thermal expansion of the bulk lattice.[11] In a related work we have examined briefly the case of descent from a ⟨110⟩ step edge on Ag(100).[12] These initial studies have provided the basis for a full theoretical study of the processes that control growth and diffusion at these surfaces.

Our goal in this paper is to investigate homoepitaxial growth on Ag(100) by examining the temperature dependence of the diffusion coefficients for adatom motion on its

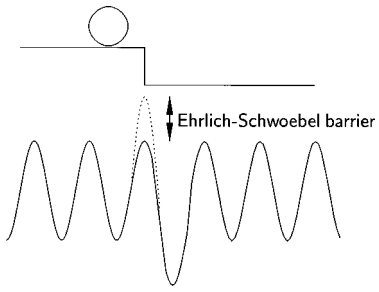

FIG. 1. Sketch of a potential energy surface for step descent with an Ehrlich-Schwoebel barrier.

flat terraces, for those along the ⟨110⟩ and ⟨100⟩ step edges, and for descent from these two types of steps which are found in experiments.[13,14] To get as complete a picture as is currently possible, we consider both exchange and hopping mechanisms for self-diffusion and examine their relative importance, as a function of surface temperature. For microscopic details of growth processes and for insights into available experimental data, we also calculate barriers for several diffusion paths in the neighborhood of the two types of step edges and explore the preferences for an adatom for approaching them. On this subject some insightful initial work, using *ab initio* electronic structure calculations, already exists. In these calculations Yu and Scheffler[15,16] have mapped out the one-dimensional potential energy surface for self-diffusion on the ⟨110⟩ step edge and flat terraces of Ag(100), and have calculated the static-lattice activation barriers for diffusion using both the local density (LDA) and generalized gradient (GGA) approximations in density-functional theory. Through comparisons of the static energy barriers, they conclude: (1) on Ag(100) terraces hopping is more favorable than exchange; (2) along the ⟨110⟩ step edge the activation barrier for hopping is small; and (3) for descent from the ⟨110⟩ step edge the barrier for exchange is about the same as that for hopping on the flat terrace. These results for the energy barriers provide good rationale for the experimentally observed layer-by-layer growth on Ag(100). Our main point of departure from these *ab initio* results is in the inclusion of lattice vibrations in the phenomenological description of the systems. By doing so we are able to calculate the local thermodynamic quantities and thereby make our calculations applicable for a large range of temperatures, within the limits of validity of the harmonic and quasiharmonic approximation of lattice dynamics. As a result we are able to calculate activation barriers and preexponential factors for processes of interest and relate our results directly to experimental data on growth. Such finite-temperature calculations are not yet feasible with *ab initio* methods because of extensive computational demands even on the most advanced high-performance machines. We have, therefore, resorted to the usage of empirical, many-body interaction potentials which, as we shall see, reproduce the static energy barriers in reasonably good agreement with the *ab initio* results, and allow us to incorporate fully the dynamics of the systems.

The paper is organized as follows: in Sec. II we discuss briefly the interaction potentials used; in Sec. III we present the basic formalism for diffusion, including the calculation of thermodynamic functions and local vibrational density of states (LDOS); in Sec. IV we summarize the computational method; Sec. V contains the results and discussion, in the context of previous experimental and theoretical work; in Sec. VI we present our conclusions.

II. INTERACTION POTENTIALS

The interaction potential and the force constant matrix required to calculate the LDOS are derived by using two different sets of embedded atom method (EAM) potentials:[17] one by Foiles, Daw, and Baskes (FDB) (Ref. 18) and the other by Voter and Chen (VC).[19] This allows us to estimate the dependence of our results on the peculiarities of the interaction potential. In the framework of the EAM, the total energy of a metal is given as a sum of an embedding function and an electrostatic energy contribution due to core-core overlap. The embedding function is defined as the energy needed to embed an atom in the local homogeneous electron density as provided by the other atoms of the metal. The electron density is approximated by the superposition of atomic-electron densities. The functions of the EAM are determined empirically by fitting the predicted results to the equilibrium density, sublimation energy, elastic constants, vacancy-formation energy, and, in the case of the VC potential, to also the bond strength, and bond length of the diatomic molecule. Among other attributes, the FDB potentials provide accurate and detailed description of the lattice dynamics of the Ag, Cu, and Ni surfaces.[20–24] The resulting surface phonon frequencies at the high-symmetry points in the Brillouin zone, for several surfaces of Ag and Cu, are also found to be in excellent agreement with first-principles calculations.[25] Further, a systematic study of surface self-diffusion[26] showed that the general trend for activation energies calculated with EAM potentials for the low-Miller-index surfaces of Ni, Cu, Al, Ag, Au, Pd, and Pt are consistent with experimental observations. From the quantities to which the different EAM functions are fitted one would expect the VC potential to be more realistic for studies of adatoms on surfaces. On the other hand, as already mentioned, the FDB potential works very well for vibrational properties at surfaces. It is thus not trivial to decide, *a priori*, which EAM potential is more suitable for calculations of the contributions of lattice vibrations to self-diffusion on flat and stepped Ag(100) surfaces. We use here both potentials and compare the results to experimental and other theoretical results where available. As we shall see, activation barriers obtained from either EAM potential are in agreement with those extracted from *ab initio* calculations based on either LDA or GGA, and that both types of calculations lead to similar ambiguities in the results. It is thus not possible, even with availability of *ab initio* calculations, to choose between the two EAM potentials vís-a-vís the issues addressed in this work.

III. BASIC FORMALISM

The basic formalism for diffusion, including the calculation of the thermodynamic functions and the LDOS, has been described in detail in earlier publications.[11,12] Here we give a short summary of the main equations. For an isolated atom migrating on a surface, the *intrinsic*[27,28] diffusion coefficient D may be obtained from the Einstein relation for random walk, $D=\langle \Delta r^2 \rangle / 2\alpha t$, where $\langle \Delta r^2 \rangle = N l^2$ is the mean-square displacement of the diffusing particle during the time period t, α is the dimensionality of the motion, and l is the jump distance. The number of jumps N is the product of the time period and a hopping rate Γ, which for thermally activated diffusion may be expressed according to transition-state theory[9] as

$$\Gamma = \frac{k_B T}{h} \exp\left(\frac{-\Delta F}{k_B T} \right), \tag{1}$$

where, ΔF is the difference in the Helmholtz free energy between the maximum (saddle point) and the minimum of the potential-energy curve. The essential feature in Eqs. (1)

is the dependence of Γ on the free energy of activation, $F=\Phi+f_{\rm vib}$, where Φ is the structural energy of the system, and $f_{\rm vib}=U_{\rm vib}-TS_{\rm vib}$ is the vibrational free energy, with $U_{\rm vib}$ the internal energy due to vibrations and $S_{\rm vib}$ the vibrational entropy. The diffusion coefficient may now be written as

$$D=D_0(T)\exp\left(\frac{-\Delta\Phi}{k_BT}\right)$$

with

$$D_0(T)=\frac{k_BT}{h}\frac{nl^2}{2\alpha}\exp\left(\frac{\Delta S_{\rm vib}}{k_B}\right)\exp\left(\frac{-\Delta U_{\rm vib}}{k_BT}\right), \qquad (2)$$

where, $\Delta S_{\rm vib}$, $\Delta U_{\rm vib}$, and $\Delta\Phi$ are the differences in the respective quantities calculated with the adatom at the maximum, and the minimum points on the potential-energy surface, and n is the number of jump-equivalent directions available to the adatom. In the classical limit, the above form of the equation is analogous to the formulation proposed by Vineyard[29] who described an effective jump frequency for the transition rate as the ratio of the product of N normal frequencies of the system in the minimum-energy position, to N-1 normal frequencies for the system in the transition state. In previous publications we have used a slightly different expression for $D_0(T)$. There the term $\Delta U_{\rm vib}$ was included in the exponential, rather than in the preexponential, thereby highlighting the temperature dependence of the activation barriers. In most experiments the diffusion coefficients are derived from Arrhenius plots and it is not possible to measure this temperature dependence of the energy barriers. Since $\Delta U_{\rm vib}=-k_BT$, its effect is to contribute simply a multiplicative factor to $D_0(T)$, and subsequently to the diffusion coefficient.[30]

The thermodynamical quantities appearing in the above equations may be obtained from the partition function calculated within the harmonic and quasiharmonic approximation of lattice dynamics. We have for the vibrational internal energy and entropy:

$$U_{\rm vib}=k_BT\int_0^{\nu_{\max}}N(\nu)\left(\frac{1}{2}x+\frac{x}{e^x-1}\right)d\nu$$

$$S_{\rm vib}=k_B\int_0^{\nu_{\max}}N(\nu)\left(-\ln(1-e^{-x})+\frac{x}{e^x-1}\right)d\nu, \qquad (3)$$

where $x=h\nu/k_BT$, and $N(\nu)$ is the density of phonon states as a function of frequency ν. The notable quantity here is the vibrational density of states which can be written as $N(\nu)=\Sigma_l n_l(\nu)$, where $n_l(\nu)$ is the local density of states in region l. Depending on the location of the adatom on the surface, it encounters particular LDOS which, as we shall see, are strikingly different for the transition state and the minimum-energy positions and lead to the differences in the local thermodynamic functions in these two regions. To calculate the LDOS we diagonalize the force constant matrix that yields the eigenvalues (ν) and eigenvectors (u). The local vibrational density of states at the site l in the direction β is calculated as

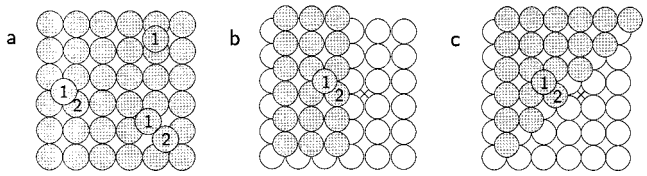

FIG. 2. Top view for diffusion on flat Ag(100) via hopping and exchange: (a) adatom in the fourfold (minimum-energy) position (left) and in the transition state (right) for the hopping process (above: twofold bridge position) and for the exchange process (below); initial geometry for descent from (b) a ⟨110⟩ step; (c) a ⟨100⟩ step.

$$n_{l,\beta}(\nu)=\sum_i^N\frac{\alpha}{\pi}|u_{l,\beta}(\nu_i)|^2e^{-\alpha^2(\nu-\nu_i)^2}, \qquad (4)$$

where α governs the width of the δ function. The sum is over all eigenvalues ν_i, where N is the total number of eigenvalues.

IV. METHOD OF CALCULATION

The diffusion processes and paths to be investigated in this paper are sketched in Figs. 2 and 3. Figure 2(a) shows a top view for diffusion on the flat Ag(100) surface via hopping and exchange. On the left of the figure the adatom is shown in the fourfold (minimum-energy) site. At the right the two different transition states are indicated: twofold bridge site (above) for the hopping process; the two atoms (below) for exchange. During the hopping process the adatom labeled (1) jumps from its minimum-energy position, over the bridge, into its new minimum-energy position, which is equivalent to the position shown in Fig. 2(a). In the exchange process a surface atom labeled (2) and the adatom (1) move in a concerted motion towards the transition state and finally the surface atom (2) becomes an adatom occupying a minimum-energy position and the former adatom (1) sits in the previous position of atom (2). Figures 2(b) and 2(c) show the initial geometries for descent from a ⟨110⟩ and a ⟨100⟩ step, respectively. The cross in Figs. 2(b) and 2(c) represents the final position the adatom would occupy if it hops from the respective step edge to the terrace below. For the exchange process the step atom labeled (2) moves towards the position marked by the cross and the adatom labeled (1) moves into the step edge position of atom (2). In Fig. 3, for the ⟨110⟩ and ⟨100⟩ step edge geometries, four diffusion paths for the hopping of an adatom are indicated by the arrows labeled I–IV. Path I indicates hopping parallel to the respective step edges, path II shows diffusion away from the ascending steps, path III marks diffusion parallel to de-

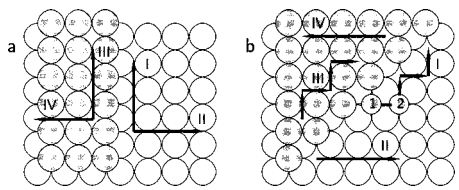

FIG. 3. Step edge geometries for (a) ⟨110⟩ step and (b) a ⟨100⟩ step. The arrows I–IV indicate paths for adatom diffusion via hopping.

scending steps, and path IV indicates in both cases diffusion away from a descending step. In Fig. 3(b) the positions marked with 1 and 2 are two nonequivalent minimum-energy positions in the neighborhood of an ascending ⟨100⟩ step.

The force constant matrices for atomic configurations along the diffusion path (minimum energy and transition state) were evaluated from derivatives of the interaction potentials with all atoms relaxed in their minimum-energy configuration as obtained by minimization of the total energy using a conjugate gradient technique in the $3N$-dimensional coordinate space, where N is the number of atoms in the cell. To determine the transition-state configurations we moved adatom (1) for hopping processes, and in addition the terrace or step edge atom (2) for exchange processes, in small increments towards their final positions and allowed all atoms to relax each time. To keep adatom (1), and the terrace or step edge atom (2), from returning to their minimum-energy positions, and to prevent the whole crystal from moving relative to these positions, we fixed the positions of these atoms and of the eight edge atoms of the cubic cell, in the direction of the reaction coordinate, and allowed the minimization of the total energy to proceed in the $3N$-9−dimensional coordinate space. The configuration with the highest potential energy is that of the transition state. The static lattice activation barrier, $\Delta\Phi$, is then the difference in the total energy calculated for the maximum and the minimum points on the energy-position curve. Note that for diffusion parallel to the ⟨100⟩ step [path I in Fig. 3(b)] exchange processes involving a step edge atom and an adatom located in position 1 may seem plausible for geometric reasons. However, regardless of whether we move a step edge atom out of its position or the adatom towards the step edge atom, no concerted exchange process was seen to occur. In the first case, the step edge atom ends up in a position equivalent to that of the adatom, while the latter remains in its original position. In the second case, the adatom ends up in the step edge position and the step edge atom jumps on top of the step edge, which is a concerted exchange process but for step ascent.

The substrate is build by (10×10) atoms in the x-y plane and 10 layers for the flat surface geometry. The size of the system is then large enough that the LDOS do not exhibit any significant finite-size effects. To create the substrate with a step, an additional 1/2 layer was put on the (100) surface. Periodic boundary conditions were applied in the x and y direction, to remove edge effects from the LDOS. For hopping processes we calculate the LDOS for the adatom (1) both in the minimum energy position, and in the transition state. For exchange processes the LDOS is calculated as the sum of the LDOS for the two moving atoms, i.e., for adatom (1) and the terrace or the step edge atom (2), both for the minimum-energy and the transition-state configurations.

The technique described so far invoke the harmonic approximation in the calculation of the force constant matrices. Majority of the results presented here are obtained with this approximation and are suitable for quite a large range of temperatures. Previous work on several metal surfaces has shown that the harmonic/quasiharmonic approximation remains valid to about half the bulk melting temperature, beyond which enhanced anharmonic effects become significant.[22,23,31] Our experience with molecular dynamics simulations of Ag(100)[22] and subsequent examination of the temperature variation of the mean-square vibrational amplitudes shows that the harmonic approximation may be pushed to about 450 K–500 K [bulk melting temperature for Ag with EAM potentials is 1170 K (Ref. 32)]. For higher temperatures, the quasiharmonic approximation should be used. In the quasiharmonic theory for surfaces,[33] the system is allowed to expand both in the bulk and at the surface, and the force constant matrix is calculated in the thermally averaged positions of the atoms. In principle, these mean position of the surface atoms may be obtained from a molecular-dynamics simulation of the system, at the desired temperature, having the bulk lattice constant appropriate for that temperature. In practice, however, this is a formidable task in the case of the system with the adatom in the equilibrium position (fourfold site), and an impossible one with the adatom in the transition state. Since we would like to explore the effect of thermal expansion on the activation barriers and prefactors for surface diffusion, we have proceeded here with a modified version of the quasiharmonic theory, which is feasible but limited in application to special cases. Our approximation involves inclusion of thermal expansion in the bulk, and in the surface plane, but not in the direction normal to the surface. On Ag(100), at 600 K, for which we have performed these ''quasiharmonic'' calculations, the surface thermal expansion is small and our procedure below for obtaining the force-contant matrices is reasonable. This method would not be suitable for higher temperatures, or for systems with large surface thermal expansion at the desired temperature. With these comments in mind we give details of the calculations performed at 600 K (''quasiharmonic'').

For calculations in the quasiharmonic approximation we first determined the lattice constant at the particular temperature using molecular-dynamics (MD) simulations. This was done by allowing the bulk system, consisting of 1000 atoms per cell, to evolve over 10 ps under conditions of constant pressure (0 bar) and constant temperature (for each potential). From the thermal expansion of the MD cell we determined the lattice constant, at the desired temperature, and used it to generate the system with (100) surface orientation plus an adatom. This system was allowed to relax to its minimum-energy configuration (in the expanded MD cell), as described above, and the force constant matrix and activation barrier $\Delta\Phi^{\text{quasi}}$ calculated at the particular temperature.

V. RESULTS AND DISCUSSION

In this section we first examine the striking features and the peculiarities of the calculated vibrational density of states with the adatom/accompanying atom in the specific sites on Ag(100) terrace, and at and near the ⟨100⟩ and ⟨110⟩ step edges. This is followed by a discussion of the results for the energy barriers, the preexponential factors for hopping and exchange processes, and the Arrhenius plots for adatom diffusion on flat Ag(100). The thermodynamic functions, Schwoebel barriers, and the calculated preexponential factors for descent from the ⟨100⟩ and ⟨110⟩ step edges are presented in Sec. V C, together with a discussion of the implications for growth on Ag(100). Finally, the potential-energy surface and diffusion via hopping in directions parallel and perpendicular to the two types of step edges are explored in Sec. V D.

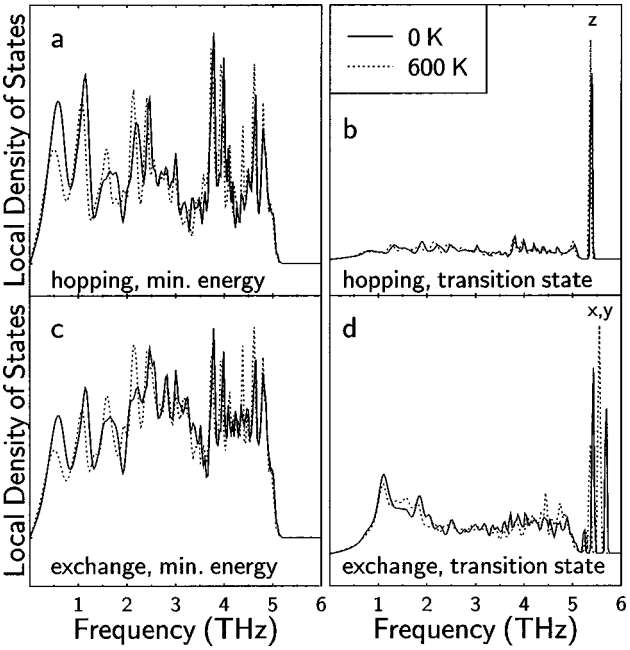

FIG. 4. LDOS for the moving atoms on flat Ag(100) calculated with the lattice constant for 0 K (solid line); for 600 K (dotted line), using the FDB potential: (a) adatom in the minimum-energy position, (b) adatom in the transition state for hopping, (c) adatom and surface atom in the minimum-energy position, (d) adatom and surface atom in the transition state for exchange.

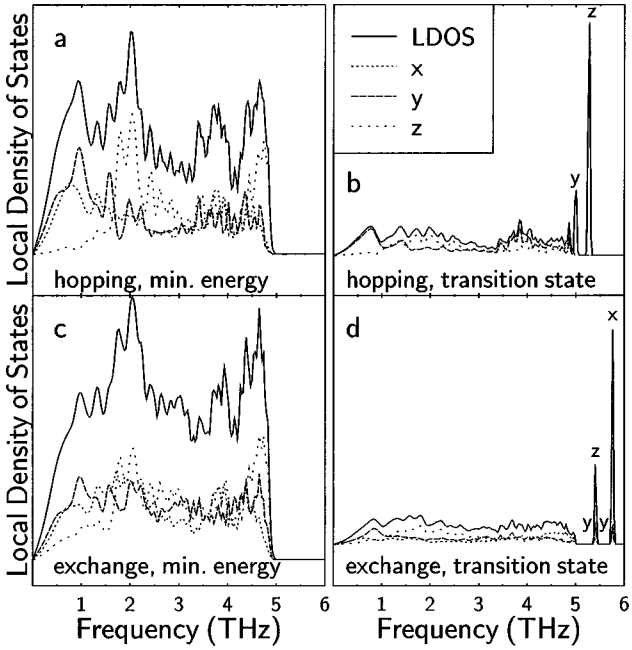

FIG. 5. LDOS and their x, y, and z components for descent from a ⟨110⟩ step edge: (a) adatom in the minimum energy position, (b) adatom in the transition state for hopping, (c) adatom and step edge atom in the minimum-energy position, (d) adatom and step edge atom in the transition state for exchange. All curves are calculated using the VC potential.

A. Vibrational properties

In Fig. 4, the LDOS for the moving atoms (adatom for hopping, adatom plus terrace atom for exchange, as discussed above) in the minimum-energy and the transition-state positions are shown, for both diffusion mechanisms on flat Ag(100). These LDOS are calculated using the FDB potential. The solid lines represent the LDOS for a crystal at 0 K (lattice constant: $a_o = 4.09$ Å), while the dotted lines show the results for an expanded lattice at 600 K ($a_o = 4.13$ Å). For both mechanisms we find a broad frequency distribution for the LDOS for moving atoms in the minimum energy positions [Figs. 4(a) and 4(c)]. These broad frequency distributions are quite different as compared to the LDOS for an Ag atom in the bulk or on the (100) surface.[11,12] For the LDOS calculated for the moving atoms in transition state positions [Figs. 4(b) and 4(d)] the most striking features are narrow peaks at high frequencies. For hopping processes, the high-frequency mode is contributed exclusively by a vibration in the z direction (perpendicular to the surface), while for exchange processes the high-frequency modes arise mainly from vibrations in the xy plane. The LDOS for the moving atoms in the transition state possess one vibrational degree of freedom less than those for the respective minimum-energy configurations, in accordance with transition-state theory. A comparison of the LDOS at 0 K and the corresponding one at 600 K shows only slight differences for both processes. In Fig. 4(d), the highest-frequency mode is shifted slightly towards lower frequencies at higher temperatures, otherwise the LDOS are very similar. The LDOS obtained using the VC interaction potential display very similar features to the ones presented in Fig. 4.

In Figs. 5 and 6 the LDOS and their x, y, and z components for the moving atoms for step descent (adatom for hopping, adatom and step edge atom for exchange) via hopping and exchange from a ⟨110⟩ and a ⟨100⟩ step, respec-

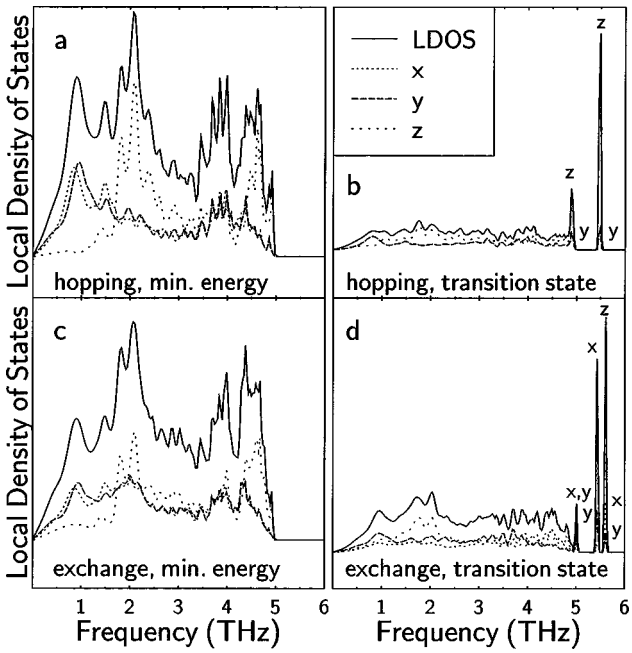

FIG. 6. LDOS and their x, y, and z components for descent from a ⟨100⟩ step edge. (a) adatom in the minimum-energy position, (b) adatom in the transition state for hopping, (c) adatom and step edge atom in the minimum-energy position, (d) adatom and step edge atom in the transition state for exchange. All curves are calculated using the VC potential.

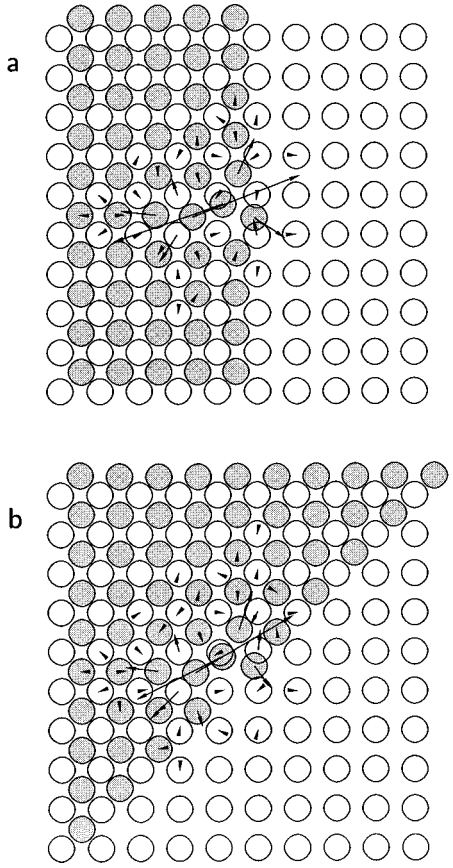

FIG. 7. Displacement pattern for the high-frequency mode (a) at $\nu = 5.65$ THz in Fig. 5(d), (b) at $\nu = 5.44$ THz in Fig. 6(d).

tively, are shown. These LDOS are calculated using the VC potential but the corresponding results obtained with the FDB potential are similar, and their general features are analogous to the ones shown in Fig. 4. Note that the z components in Figs. 5(a), 5(c), 6(a), and 6(c) have major weight at higher frequencies as compared to the x and y components. The major weight of the LDOS for the moving atoms in their transition-state positions are again shifted towards higher frequencies, due to the existence of additional high-frequency modes. The polarization of the high-frequency peaks is indicated in Figs. 5(b), 5(d), 6(b), and 6(d).

In Figs. 7(a) and 7(b) we show the displacement pattern for the high-frequency mode at $\nu = 5.65$ THz in Fig. 5(d) and for the mode at $\nu = 5.44$ THz in Fig. 6(d), respectively. Both modes have vibrations in the xy plane. The length of the arrows in Fig. 7 is proportional to the magnitude of the displacement. The atoms for which only the tip of the arrow is shown have displacements only a few percent of the largest displacement. Displacements less than 0.5% of the largest one are not indicated. As one can see from Fig. 7, these high-frequency modes are highly localized in the vicinity of the two moving atoms—a feature common to all cases studied in this paper. This behavior can be explained as follows. In general, atoms occupying the transition state have lower coordination numbers as compared to the ones in the minimum-energy positions, which leads to a stronger bond between the remaining nearest-neighbor atoms, resulting in modes with higher frequencies.

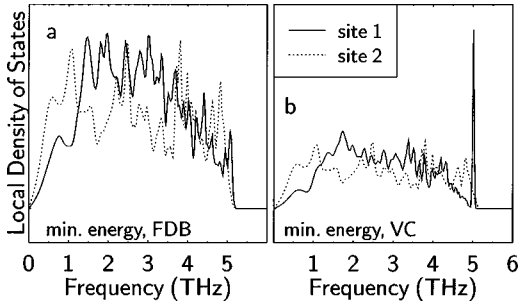

FIG. 8. LDOS for adatoms located in nonequivalent minimum energy positions 1 and 2 (Fig. 3) at the ⟨100⟩ step edge.

In Figs. 8(a) and 8(b) we compare the LDOS for adatoms in the nonequivalent minimum energy positions, indicated as 1 and 2 in Fig. 3, at the ⟨100⟩ step edge, using the FDB and VC potentials, respectively. For both potentials we find the major weight for the LDOS for the adatom in site 1, located at the step edge, to be shifted towards higher frequencies, while the total frequency range remains the same for both sites. In Fig. 8(b) the highest-frequency mode is significantly enhanced compared to the other modes, but otherwise both potentials yield the same trend. This trend can also be understood in terms of the coordination number. The coordination number for an atom at site 1 is 6 while at site 2 it is 4. The lower coordination again leads to stronger bonds and higher vibrational frequencies. The difference in the binding energy between site 1 and site 2 is 0.45 eV for the FDB, and 0.54 eV for the VC potential. We will come back to this point later.

B. Diffusion on the flat surface

From the LDOS shown in Figs. 4(c) and 4(d) for exchange on the flat surface we have calculated the vibrational thermodynamic functions, i.e., the free energy f_{vib}, the internal energy U_{vib}, and the entropy S_{vib}, which are presented in Figs. 9(a)–9(c), respectively. The lines represent the results from the harmonic approximation and the circles the ones obtained in the quasiharmonic approximation applied at 600 K. As one can see, the results from these two approximations do not differ much. The differences between the corresponding thermodynamic functions for the adatom and the terrace atom in the transition-state and in the minimum-energy position, as a function of temperature, are given in Figs. 9(d)–9(f). Once again, the circles indicate the results from the quasiharmonic approximation at 600 K. The inset in Fig. 9(f) shows the preexponential factor D_0 as a function of temperature. It is almost constant. As for the negative values for ΔS_{vib}, they arise from two different factors affecting the adatom (and the terrace atom in the exchange process) in the minimum-energy and the transition-state locations: the difference in the number of vibrational degrees of freedom, and the shift in the major weight of the LDOS to higher frequencies. The contribution of ΔS_{vib} overcompensates the contribution of ΔU_{vib} leading to a significant increase of the vibrational activation free energy of up to 105 meV (at 600 K), as seen in Fig. 9(d). Similar trends were found for hopping processes.[11] Once again, for both mechanisms we find only small differences between the thermodynamic functions that are calculated in the harmonic and in the quasiharmonic approximation.

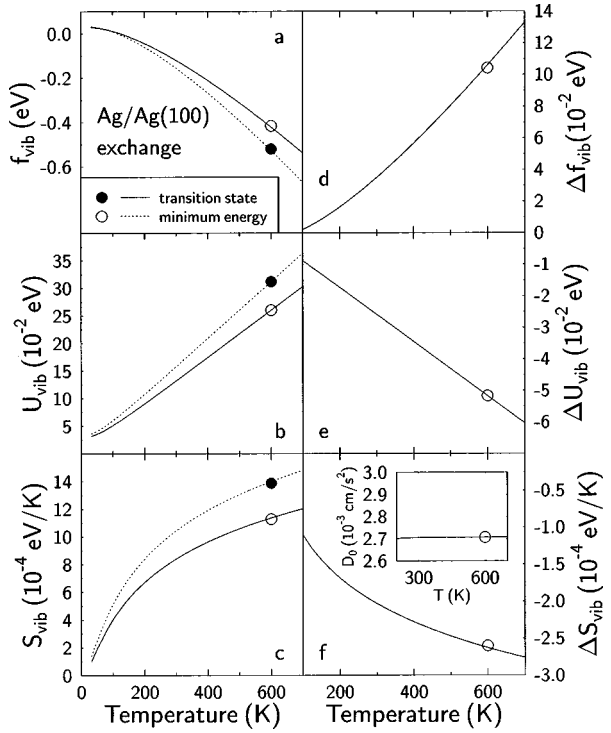

FIG. 9. The vibrational thermodynamic functions for the adatom and the surface atom in the minimum energy and the transition state for exchange on the flat surface. The quantities were calculated with the FDB potential. The lines show results in the harmonic approximation and the circles those in the quasiharmonic approximation.

Our results for the activation barriers $\Delta\Phi$ and the preexponential factors D_0, for both diffusion mechanisms, for the FDB and VC potential, using the harmonic and quasiharmonic approximation, together with results for $\Delta\Phi$ calculated from first principles[15] and also an experimentally (low-energy ion scattering) obtained value,[34] are summarized in Table I. Here we find the barrier calculated with the FDB potential for exchange to be in better agreement with the *ab initio* results. Based on just the values for $\Delta\Phi$ in the table, hopping processes would be favored, in agreement with previous work using EAM potentials.[26] It is interesting to note that the thermal expansion of the lattice causes an increase of the activation barrier for hopping [+0.01 eV (FDB), +0.02 eV (VC)], but a decrease for exchange [−0.06 eV (FDB), −0.07 eV (VC)]. Especially for the VC potential, the barriers at 600 K for hopping and exchange are very close (difference: 0.02 eV), which implies that at higher temperatures exchange processes may become almost as important as hopping, on flat Ag(100). The preexponential factors (which contain ΔS_{vib} and ΔU_{vib}) in Table I seem reasonable when compared with intuitive values that have generally been assumed.[35] Vibrational entropy contributions have a dramatic effect on the preexponential factor [at 600 K, for example, $\exp(\Delta S/k)\approx 0.05$]. The net effect of all terms, however, is to make the preexponential factor almost temperature independent, as expected in the classical limit.[30] From the tables we see that for both potentials, and within the harmonic and quasiharmonic approximations, the preexponential factors for exchange processes are always higher than those for hopping. Together with the lowering of the barriers, this effect would suggest that exchange processes become more important at higher temperatures. Figure 10 shows the Arrhenius plots for self-diffusion via hopping and exchange on Ag(100), calculated with both potentials. For the VC potential, in particular, one can see clearly that the diffusion coefficients for both mechanisms calculated in the quasiharmonic approximation are more similar than those obtained by neglecting the thermal expansion of the lattice.

Ever since the first observation of exchange mechanism on an isotropic surface by De Lorenzi and Jacucci,[36] it has become evident that self-diffusion on (100) surfaces of Al, Pt, and Ir occurs dominantly via exchange.[37,38] For self-diffusion on Cu(100) and Ag(100) there has been some debate about the relevant mechanism. Static calculations based

TABLE I. Diffusion on the flat surface: activation barriers $\Delta\Phi$ calculated at 0 K (harmonic approximation) and for the expanded system at 600 K (quasiharmonic approximation), and the corresponding preexponential factors. The *ab initio* results* were calculated by Yu and Scheffler and the experimental barrier was obtained by Langelaar, Breeman, and Boerma.

Process	$\Delta\Phi$ (eV)	D_0 (cm^2/s)
Harmonic approximation:		
hop, FDB	0.48	8.1×10^{-4}
hop, VC	0.48	2.3×10^{-3}
exch, FDB	0.78	2.7×10^{-3}
exch, VC	0.59	3.5×10^{-3}
hop, LDA*	0.52	
hop, GGA*	0.45	
exch, LDA*	0.93	
exch, GGA*	0.73	
Quasiharmonic approximation at 600 K:		
hop, FDB	0.49	9.3×10^{-4}
hop, VC	0.50	1.5×10^{-3}
exch, FDB	0.72	2.7×10^{-3}
exch, VC	0.52	2.1×10^{-3}
experiment	(0.45±0.05), 160 K	

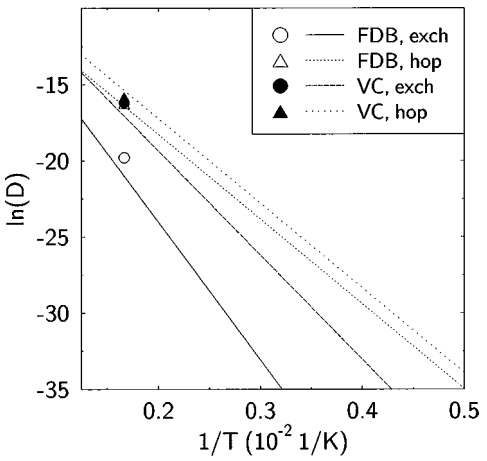

FIG. 10. Arrhenius plots for hopping and exchange mechanisms, calculated using the FDB and the VC potential. The lines show the results in the harmonic approximation and the symbols the ones in the quasiharmonic approximation.

on the effective medium theory had predicted exchange to be the dominant diffusion process on Cu(100),[39] but most previous work based on EAM potentials,[26] as well as on *ab initio* calculations,[15,40] favored hopping for Cu and Ag. The present study for Ag/Ag(100) reveals that the relative importance of hopping and exchange processes changes with temperature.

C. Step descent from ⟨110⟩ and ⟨100⟩ steps

The vibrational contribution to the activation free energy $\Delta f_{\rm vib}$, activation internal energy $\Delta U_{\rm vib}$, and activation entropy $\Delta S_{\rm vib}$ for descent from a ⟨110⟩ and a ⟨100⟩ step edge, for hopping and exchange processes, calculated in the harmonic approximation, are shown in Fig. 11. Quite clearly the vibrational contributions to the respective quantities are very similar for both mechanisms, as well as, for both types of steps. The curves in Fig. 11 are calculated using the VC potential, but for the FDB potentials we obtain similar results. Our calculated values for the activation barriers (at 0 K), the Ehrlich-Schwoebel barriers and the preexponential factors for both mechanisms, obtained from both types of EAM potentials, are summarized in Table II. Comparison is also made with barriers for descent from a ⟨110⟩ step obtained from *ab initio* calculations.[15] For the descent from a ⟨110⟩ step, activation barriers from the VC potential show exchange to be energetically favored over hopping, while the FDB potential shows those for hopping to be somewhat lower. The trend and the values for the barriers obtained with the VC potential are in good agreement with the *ab initio* calculations,[15] although the results from the *ab initio* calculations are by no means unequivocal since LDA and GGA versions of the calculations yield somewhat different results. Unlike the case of the flat surface, for descent from a ⟨110⟩ step the VC potential yields more realistic results. For the ⟨100⟩ step edge, on the other hand, the barriers for step descent, from both EAM potentials are similar and those for exchange are significantly lower than those for hopping. These barriers for exchange are also significantly lower than all barriers for descent from the ⟨110⟩ step edge. As shown in Table II, the VC potential also yields for both types of steps,

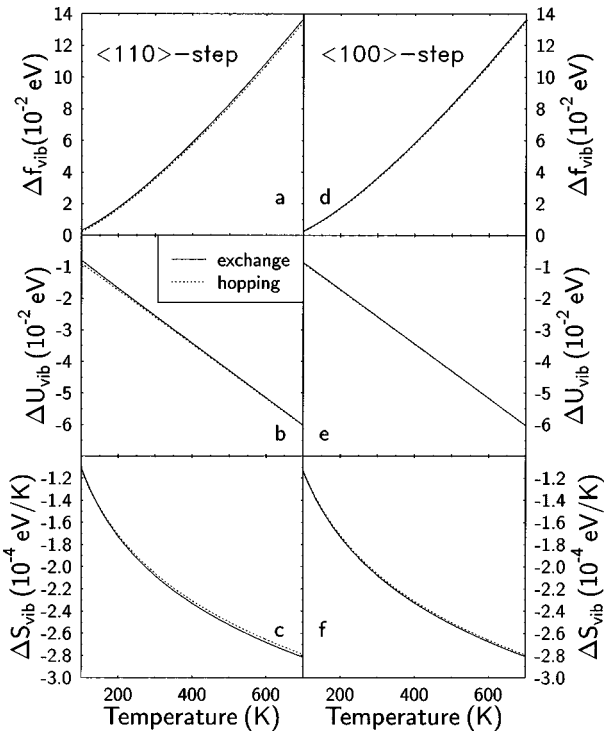

FIG. 11. The activation vibrational free energy $\Delta f_{\rm vib}$, internal energy $\Delta U_{\rm vib}$, and entropy $\Delta S_{\rm vib}$ for descent via hopping and exchange from a ⟨110⟩ and a ⟨100⟩ step edge. The quantities were calculated with the VC potential.

for both mechanisms, the same preexponential factor for step descent, while we find a higher value for D_0 for exchange (factor 2–3) from the FDB potential. These results indicate that exchange from the ⟨100⟩ step edge provides a path for interlayer diffusion on Ag(100) with a very low activation barrier. In fact, it is a path with a negative Ehrlich-Schwoebel barrier. In a previous work Teichert and co-workers[13] have investigated the development of the morphology of an Ag(100) single-crystal surface, bombarded with 600 eV Ar^+ ions and during homoepitaxial growth with

TABLE II. Step descent: activation barriers $\Delta\Phi$, corresponding Ehrlich-Schwoebel barriers (ESB), and the preexponential factors. The *ab initio* results* were calculated by Yu and Scheffler.

Process	$\Delta\Phi$ (eV)	ESB (meV)	D_0 (cm^2/s)
⟨110⟩ step:			
hop, FDB	0.59	110	2.7×10^{-3}
hop, VC	0.70	220	3.3×10^{-3}
exch, FDB	0.64	160	8.4×10^{-3}
exch, VC	0.51	30	3.3×10^{-3}
hop, LDA*	0.70	180	
hop, GGA*	0.55	100	
exch, LDA*	0.52	0	
exch, GGA*	0.45	0	
⟨100⟩ step:			
hop, FDB	0.51	30	2.7×10^{-3}
hop, VC	0.55	70	3.3×10^{-3}
exch, FDB	0.38	−100	5.4×10^{-3}
exch, VC	0.31	−170	3.3×10^{-3}

deposition rates of 1 and 2 ML per minute at 170 K and 300 K, using spot profile analysis of low electron energy diffraction (SPA-LEED). The authors also performed Monte Carlo (MC) simulations of diffusion via hopping using pairwise additive Morse potentials, to understand the variations of spot shapes with temperature. Their results predict the barrier for descent from the ⟨100⟩ step to be smaller than that for the ⟨110⟩ step. They also conclude that under conditions of ion bombardment and homoepitaxial growth both types of steps occur with the same frequency at 170 K, but there is a preference for the ⟨110⟩ steps at 300 K. Their result is consistent with scanning tunneling microscopy (STM) experiments,[14] in which Ag islands with a square shape and commonly rounded corners were observed at room temperature on Ag(100). A previous theoretical study for Ag(100) based on EAM potentials, however, shows the ⟨110⟩ steps to be energetically favored over the ⟨100⟩ steps[41] at 0 K. These authors find the energy per unit length to be about a factor $\sqrt{2}$ larger for the ⟨100⟩ step than for the ⟨110⟩ step. This result was recently corroborated by *ab initio* calculations,[16] which predict the equilibrium shape of Ag islands on Ag(100) to be octagonally shaped with an edge-length ratio for the ⟨110⟩ and ⟨100⟩ step edges as 10:3, consistent with the experimental results.[14] At 300 K, we find from our activation barriers that the jump frequency is more than three orders of magnitude higher for descent from a ⟨100⟩ step edge than from a ⟨110⟩ step. This leads us to the conclusion that the dominant path for interlayer diffusion on Ag(100) is descent via exchange from the ⟨100⟩ step edge.

D. Diffusion parallel and perpendicular to ⟨110⟩ and ⟨100⟩ step edges

To explore possible preferences for approaching a particular type of step edge, we have calculated the activation barriers for diffusion parallel and perpendicular to ⟨110⟩ and ⟨100⟩ step edges. The paths considered are labeled in Fig. 3 as I–IV. For all barriers along the diffusion paths III and IV, we found values which are very close (± 0.02 eV) to the barriers for diffusion on the flat surface. Thus, we do not find any preference to approach either type of descending steps on Ag(100). In Figs. 12(a) and 12(b), we show the potential energy surfaces, along paths labeled II in Figs. 3(a) and 3(b), for approaching an ascending ⟨110⟩ and ⟨100⟩ step edge, respectively. The distance 0 Å corresponds to the fourfold site closest to the respective step edge. The dotted line shows the potential-energy surface for diffusion on a flat surface. For both types of steps we find that the site closest to the step edge is significantly more stable than the minimum-energy positions for adatoms on the flat surface. As mentioned earlier, this can be understood in terms of a higher coordination number at the step edge. To diffuse away from these positions along path II towards the flat surface the atoms have to overcome an activation barrier of 0.75 eV (0.69 eV, FDB) and 0.78 eV (0.73 eV, FDB) for the ⟨110⟩ and ⟨100⟩ step, respectively. For the ⟨110⟩ step edge *ab initio* electronic structure calculations using GGA predict this barrier to be 0.76 eV, while usage of LDA leads to a value of 0.96 eV. To diffuse towards the ascending step we find a lower barrier than for diffusion on the flat surface when the adatom is separated 2.89 Å from the step edge. This behavior is much more pronounced for the ⟨100⟩ step. The activation barriers

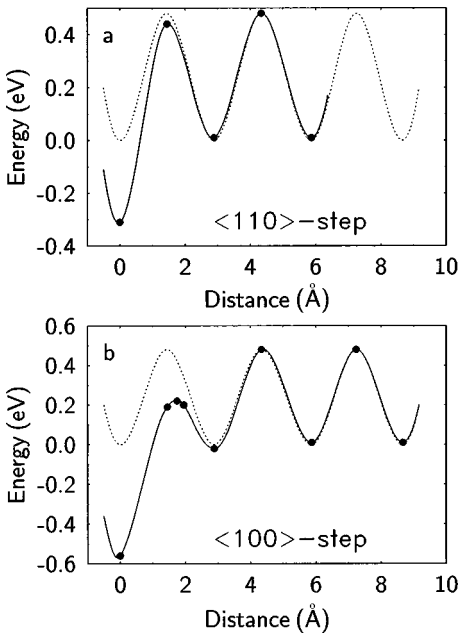

FIG. 12. Potential-energy surfaces using the VC potential for diffusion via hopping along the paths labeled II in Figs. 3(a) and 3(b), for the ⟨110⟩ and the ⟨100⟩ step, respectively.

are 0.43 eV (0.46 eV, FDB) and 0.24 eV (0.28 eV, FDB) for the ⟨110⟩ and ⟨100⟩ steps, respectively. These features of the potential-energy surfaces in the vicinity of an ascending step edge are similar to the theoretical results for Pt(111) (Ref. 42) and to experimental results for Ir(111).[43] They are also in accordance with conclusions drawn from molecular-dynamics simulations for vacancy diffusion on Ag(111).[44] The activation barriers and the preexponential factors for diffusion parallel to the ⟨110⟩ and ⟨100⟩ steps, via hopping, are shown in Table III, together with the *ab initio* results[15] that are available. The corresponding diffusion paths are labeled as I in Fig. 3. The abbreviation $(1\rightarrow 2)$ in Table III refers to diffusion from site 1 to site 2 in Fig. 3(b). As one can see from the barriers, atoms located at the ⟨110⟩ step edge have a high mobility parallel to the step edge, while atoms located at the ⟨100⟩ step edge have to overcome a high barrier. The different mobilities along the two types of step edges might support reaching thermal equilibrium. Atoms located at ⟨110⟩ step edges are very mobile, which leads first to smooth ⟨110⟩ steps. An atom which reaches a corner between a ⟨110⟩

TABLE III. Diffusion via hopping parallel to step edges: activation barrier $\Delta\Phi$ calculated at 0 K and preexponential factors D_0. The *ab initio* results* were obtained by Yu and Scheffler.

Diffusion path	$\Delta\Phi$ (eV)	D_0 (cm^2/s)
along ⟨110⟩ step, FDB	0.26	1.5×10^{-3}
along ⟨110⟩ step, VC	0.26	1.8×10^{-3}
along ⟨110⟩ step, LDA*	0.30	
along ⟨110⟩ step, GGA*	0.27	
⟨100⟩ step, $1\rightarrow2$, FDB	0.73	1.1×10^{-3}
⟨100⟩ step, $2\rightarrow1$, FDB	0.28	7.3×10^{-4}
⟨100⟩ step, $1\rightarrow2$, VC	0.78	1.1×10^{-3}
⟨100⟩ step, $2\rightarrow1$, VC	0.24	8.4×10^{-4}

and ⟨100⟩ step is more likely to stick at the ⟨100⟩ step. Atoms which descend from a ⟨100⟩ step also get caught at the step edge. Thus the ⟨100⟩ steps might get filled and become shorter. It will be interesting to pursue these processes with Monte Carlo simulations. In Table III, for diffusion parallel to the ⟨100⟩ step we find higher preexponential factors for jumps from site 1 to site 2, than for jumps from site 2 to site 1. Since the bridge positions in both cases are equivalent, this difference is solely due to the shift in the major part of weight in the LDOS for the adatoms located in the nonequivalent minimum-energy positions 1 and 2 as shown in Fig. 8. The major weight in the LDOS for atoms in site 1 is shifted towards higher frequencies, compared to the LDOS in site 2. Therefore the differences in the thermodynamic functions for an atom in site 1 and the transition state is smaller than the corresponding differences for an atom in site 2, which leads to a higher activation entropy in the former case and, therefore, to higher preexponential factors.

VI. CONCLUSION

In this paper we have investigated diffusion mechanisms that are relevant to homoepitaxial growth on Ag(100). We have calculated diffusion barriers and preexponential factors along several paths for hopping and exchange processes on the flat surface and on surfaces with ⟨110⟩ and ⟨100⟩ steps. The local thermodynamic functions were calculated from vibrational density of states within the harmonic and, at 600 K, in a modified quasiharmonic approximation. We show that at 600 K the local vibrational density of states, and hence the thermodynamic functions, calculated within these two approximations differ only slightly. In all cases considered these LDOS for atoms located in the transition state contained high-frequency peaks arising from highly localized modes. We show that the striking differences in the LDOS for the adatom in the transition-state and in the minimum-energy position lead to entropy contributions which control the behavior of the preexponential factors. We also find that the inclusion of thermal expansion, in the manner described in the text, leads to an increase of the activation barrier for hopping on the flat surface but to a decrease of the barrier for exchange processes. For the latter, thermal expansion yields significant lowering of the activation barriers (60 meV with FDB and 70 meV with VC) at 600 K, as compared to those at 0 K. This means that for diffusion on the flat terrace exchange becomes almost as important as hopping at higher temperatures. In general, we find the preexponential factors for exchange processes to be higher or, at times, the same as those for hopping. Our examination of descent from ⟨110⟩ and ⟨100⟩ step edges reveals that the dominant path for interlayer diffusion on Ag(100) is descent via exchange from the ⟨100⟩ step edge with a negative Ehrlich-Schwoebel barrier. Our investigation of diffusion barriers along several paths in the vicinity of ascending and descending steps shows that there exists no preference to approach one type of descending steps. The potential-energy surfaces near ascending steps show in both cases a very high barrier for diffusion from the step edge towards the terrace but a lower barrier to approach the step edge, as compared to barriers on the flat surface. Finally, we find low barriers for diffusion parallel to an ascending ⟨110⟩ step but high barriers for diffusion along the ⟨100⟩ step with possible consequences for the island shapes on this surface.

The usage of two different types of EAM potentials show that, in general, they lead to similar trends with some differences in specifics. Activation barriers calculated with the EAM potentials lie in the same range as those calculated with two different approximations to the density-functional theory.[15] These comparisons give us confidence that our results are reliable despite the semiempirical nature of the interaction potentials.

ACKNOWLEDGMENTS

U.K. thanks the Deutsche Forschungsgemeinschaft. We thank C. Teichert and A. Kara for suggestions and valuable discussions. This work was supported in part by the National Science Foundation under K–STAR/EPSCOR project KCASC. Computations were carried out on a Convex Exemplar SMP funded in part by NSF.

[1] G. Ehrlich and F. G. Hudda, J. Chem. Phys. **44**, 1039 (1966); R. L. Schwoebel and E. L. Shipsey, J. Appl. Phys. **37**, 3682 (1966).

[2] W. C. Elliott, P. F. Miceli, T. Tse, and P. W. Stephens, Phys. Rev. B **54**, 17 938 (1996).

[3] Y. Suzuki, H. Kikuchi, and N. Koshizuka, Jpn. J. Appl. Phys. **27**, L1175 (1988).

[4] H. A. van der Vegt, H. M. van Pinxteren, M. Lohmeier, E. Vlieg, and J. M. C. Thornton, Phys. Rev. Lett. **68**, 3335 (1992).

[5] J. Vrijmoeth, H. A. van der Vegt, J. A. Meyer, E. Vlieg, and R. J. Behm, Phys. Rev. Lett. **72**, 3843 (1994).

[6] K. Bromann, H. Brune, H. Röder, and K. Kern, Phys. Rev. Lett. **75**, 677 (1995).

[7] J. A. Meyer, J. Vrijmoeth, H. A. van der Vegt, E. Vlieg, and R. J. Behm, Phys. Rev. B **51**, 14 790 (1995).

[8] T. Michely, M. Hohage, M. Bott, and G. Comsa, Phys. Rev. Lett. **70**, 3943 (1993); W. Wulfhekel, N. N. Lipkin, J. Kliewer, G. Rosenfeld, G. Comsa, L. C. Jorritsma, and B. Poelsema, Surf. Sci. **348**, 227 (1996); L. C. Jorritsma, M. Bijnagte, G. Rosenfeld, and B. Poelsema, Phys. Rev. Lett. **78**, 911 (1997).

[9] S. Glasstone, K. J. Laidler and H. Eyring, *The Theory of Rate Processes* (McGraw-Hill, New York, 1941); C. H. Bennett, in *Algorithms for Chemical Computations*, edited by R. E. Christoffersen, ACS Symposium Series, (American Chemical Society, Washington, DC, 1977); D. A. King, J. Vac. Sci. Technol. A **17**, 241 (1980).

[10] U. Kürpick, A. Kara, and T. S. Rahman, Phys. Rev. Lett. **78**, 1086 (1997).

[11] U. Kürpick and T. S. Rahman, Surf. Sci. **383**, 137 (1997).

[12] U. Kürpick and T. S. Rahman, in *Surface Diffusion: Atomistic and Collective Processes*, edited by M. C. Tringides, NATO Advanced Study Institute Series (Plenum, New York, 1997), p. 589.

[13] C. Teichert, C. Ammer, and M. Klaua, Phys. Status Solidi A **146**, 223 (1994); C. Teichert, Ph.D. thesis, Martin-Luther-Universität

Halle-Wittenberg, Germany, 1992.
[14] J.-M. Wen, S.-L. Chang, J. W. Burnett, J. W. Evans, and P. A. Thiel, Phys. Rev. Lett. **73**, 2591 (1994); J.-M. Wen, J. W. Evans, M. C. Bartelt, J. W. Burnett, and P. A. Thiel, *ibid.* **76**, 652 (1996).
[15] B. D. Yu and M. Scheffler, Phys. Rev. Lett. **77**, 1095 (1996).
[16] B. D. Yu and M. Scheffler, Phys. Rev. B **55**, 13 916 (1997).
[17] For a review about the embedded atom method and its applications see: M. S. Daw, S. M. Foiles, and M. I. Baskes, Mater. Sci. Rep. **9**, 251 (1993).
[18] S. M. Foiles, M. I. Baskes, and M. S. Daw, Phys. Rev. B **33**, 7983 (1986).
[19] A. F. Voter and S. P. Chen, in *Characterization of Defects in Materials*, edited by R. W. Siegel, R. Sinclair, and J. R. Weertman, MRS Symposia Proceedings Vol. 82 (Materials Research Society, Pittsburgh, 1986), p. 175; A. F. Voter, Proc. SPIE **821**, 214 (1987).
[20] J. S. Nelson, M. S. Daw, and E. C. Sowa, Phys. Rev. B **40**, 1465 (1989).
[21] T. S. Rahman and Z. J. Tian, J. Electron Spectrosc. Relat. Phenom. **64/65**, 651 (1993).
[22] L. Yang, T. S. Rahman, and M. S. Daw, Phys. Rev. B **44**, 13 725 (1991).
[23] L. Yang and T. S. Rahman, Phys. Rev. Lett. **67**, 2327 (1991).
[24] T. S. Rahman, in *Condensed Matter Theories*, edited by J. Clark, K. Shoaib, and A. Sadiq (Nova, New York, 1994), Vol. 9, p. 299.
[25] K. P. Bohnen and K. M. Ho, Surf. Sci. Rep. **19**, 99 (1993).
[26] C. L. Liu, J. M. Cohen, J. B. Adams, and A. F. Voter, Surf. Sci. **253**, 334 (1991).
[27] H. P. Bonzel, Landolt-Börnstein, New Series, Vol. 26, Part III (Springer-Verlag, Berlin, 1990), p. 717.
[28] R. Gomer, Rep. Prog. Phys. **53**, 917 (1990).
[29] G. H. Vineyard, J. Phys. Chem. Solids **3**, 121 (1957).
[30] Note that cases in which quantum effects are important $\Delta U_{\mathrm{vib}} \neq k_B T$, and D_0 may show a stronger temperature dependence.
[31] G. Bracco, L. Bruschi, L. Pedemonte, and R. Tatarek, Surf. Sci. **352-354**, 964 (1996).
[32] S. M. Foiles and J. B. Adams, Phys. Rev. B **40**, 5909 (1989).
[33] R. E. Allen, G. Alldredge, and De Wette, Phys. Rev. B **4**, 1648 (1971).
[34] M. H. Langelaar, M. Breeman, and D. O. Boerma, Surf. Sci. **352-354**, 597 (1996).
[35] For a review, see G. Ehrlich, Surf. Sci. **299/300**, 628 (1994); G. L. Kellogg, Surf. Sci. Rep. **21**, 1 (1994).
[36] G. De Lorenzi and G. Jacucci, Surf. Sci. **164**, 526 (1985).
[37] P. J. Feibelman, Phys. Rev. Lett. **65**, 729 (1990).
[38] G. L. Kellogg and P. J. Feibelman, Phys. Rev. Lett. **64**, 3143 (1990); C. Chen and T. T. Tsong, *ibid.* **64**, 3147 (1990).
[39] L. B. Hansen, P. Stoltze, K. W. Jacobsen, and J. K. Nørskov, Surf. Sci. **289**, 68 (1993).
[40] C. Lee, G. T. Barkema, M. Breeman, A. Pasquarello, and R. Car, Surf. Sci. Lett. **306**, L575 (1994).
[41] R. C. Nelson, T. L. Einstein, S. V. Khare, and P. J. Rous, Surf. Sci. **295**, 462 (1993).
[42] M. Villarba and H. Jónsson, Surf. Sci. **317**, 15 (1994); R. Wang and K. Fichthorn, Mol. Simul. **11**, 105 (1993).
[43] S. C. Wang and G. Ehrlich, Phys. Rev. Lett. **70**, 41 (1993).
[44] U. Kürpick, P. Kürpick, and T. S. Rahman, Surf. Sci. Lett. **383**, L713 (1997).